Journal of Photochemistry and Photobiology A: Chemistry 218 (2011) 162–173

Contents lists available at ScienceDirect

Journal of Photochemistry and Photobiology A: Chemistry

journal homepage: www.elsevier.com/locate/jphotochem

# Optical properties of pyrene and anthracene containing imidazoles: Experimental and theoretical investigations

Dhirendra Kumar, K.R. Justin Thomas*

*Organic Materials Lab, Department of Chemistry, Indian Institute of Technology Roorkee, Roorkee 247 667, India*

ARTICLE INFO

*Article history:*
Received 27 September 2010
Received in revised form 2 December 2010
Accepted 27 December 2010
Available online 31 December 2010

*Keywords:*
Imidazole
Pyrene
Anthracene
Emission
Solvatochromism
TDDFT

ABSTRACT

A series of anthracene and pyrene containing imidazole derivatives have been synthesized and characterized by spectroscopy. Optical absorption and emission properties of the imidazole derivatives were examined in different solvents of varying polarity. The absorption profile remained unchanged on increasing the solvent polarity, while the emission maxima red-shifted progressively. The solvatochromic shifts of the emission spectra were correlated with $E_T(30)$, orientation polarizability and Kamlet–Taft. A better correlation obtained for the Kamlet–Taft treatment suggested the involvement of non-specific interactions in the excited state. The TDDFT calculation results suggested a negligible contribution of charge transfer to the optical properties and more planar excited states. The pyrene containing imidazoles showed higher decomposition temperature when compared to the analogous compounds bearing anthracene. Electrochemical data revealed that the pyrene based imidazoles are electron rich than the corresponding anthracene analogs as indicated by their facile oxidation.



## 1. Introduction

In recent years, organic heterocyclic compounds such as pyridine, oxadiazole, pyrazine and imidazole have received immense attention owing to their potential use in molecular designs targeting biological and electronic applications. Imidazole is quite attractive due to their biological activities [1–3] and sensor applications [4–8]. Fused imidazole derivatives such as benzoimidazoles and phenanthroimidazoles [9–13] have also been used in the fabrication of light-emitting devices, employing them as electron-transporting layer and as sensitizers in dye-sensitized solar cells [14–18]. Imidazoles when conjugated with the triarylamines served as effective ambipolar materials [11]. Functional imidazoles have been mainly developed due to their wide optical absorption, bright luminescence and bipolar transport characteristics. There is a growing interest in the design and synthesis of imidazoles enriched with functional chromophores to enhance their optical and charge transport properties. It is also a fundamental academic curiosity to study the optical properties of the functional hybrids to understand the interaction between the different chromophores present in the molecule. Keeping this in mind we have synthesized imidazoles containing anthracene and pyrene segments. It is our hypothesis that incorporation of fluorophoric groups such as anthracene or pyrene will enhance the emission characteristics of otherwise non-emissive imidazole core.

Imidazoles containing polyaromatic hydrocarbon hybrids are interesting due to the fact that excellent emission and thermal properties of the polyaromatic hydrocarbon will add to the electron-transporting ability of the imidazole segment and result in multi-functional materials. Polyaromatic segments such as anthracene and pyrene were widely used in the development of functional materials displaying bright emission and unique charge transporting properties [19–25]. Incorporation of pyrene or anthracene in molecular materials has been demonstrated to improve the optical and thermal properties. Pyrene and anthracene segments due to their planar and rigid architecture were prone to facilitate π–π stacking and enhance charge migration in solid state. In this paper, we describe the steady state optical properties of a series of imidazoles along with their electrochemical and thermal properties. These derivatives are emitting in the blue region and display marked thermal stability. Blue-emitting materials are attractive for application in OLEDs as hosts for phosphorescent materials.

## 2. Experimental

### 2.1. Reagents and instruments

All the chemicals were commercially available and they were used without further purification. All the solvents were dried using standard methods prior to use. $^1$H NMR and $^{13}$C NMR

* Corresponding author. Tel.: +91 1332 285376; fax: +91 1332 286202.
*E-mail address:* krjt8fcy@iitr.ernet.in (K.R.J. Thomas).

1010-6030/$ – see front matter © 2010 Elsevier B.V. All rights reserved.
doi:10.1016/j.jphotochem.2010.12.018

were recorded on a Bruker AV 500 O FT-NMR spectrometer. Deuterated chloroform ($CDCl_3$), acetone-$d_6$ or dimethylsulfoxide (DMSO-$d_6$) was used as solvent and tetramethylsilane (TMS) as internal standard. UV–Vis spectra were recorded at room temperature in quartz cuvettes using Shimadzu UV-1800 spectrophotometer for cyclohexane, toluene, dichloromethane and *N*,*N*-dimethylformamide (DMF), acetonitrile and methanol solutions. Fluorescence spectra were obtained from Shimadzu RF-5301-PC spectrofluorophotometer for cyclohexane, toluene, dichloromethane, *N*,*N*-dimethylformamide (DMF), acetonitrile and methanol solutions. Quantum yield of the dyes were calculated by following standard procedure and using Coumarin-1 ($\Phi_F$ = 0.99 in ethyl acetate) or Coumarin-6 ($\Phi_F$ = 0.78 in ethanol) as reference. Corrections due to dye absorption and refractive indices of the solvents used for measurement were incorporated in the calculation. TGA-DTA-DTG measurements were performed on Perkin-Elmer (Pyris Diamond) at a heating rate of 10 °C/min under a flow of nitrogen. The electrochemical properties were investigated by cyclic voltammetry (CV) and differential pulse voltammetry (DPV) in $CH_2Cl_2$ and DMF (**2c**) by using 0.1 M tetrabutylammonium hexafluorophosphate as supporting electrolyte. The experiments were performed at room temperature with a three-electrode cell consisting of a platinum wire as auxiliary electrode, a non-aqueous $Ag/AgNO_3$ reference electrode and a glassy carbon working electrode.

### 2.2. Synthesis

The molecular structure and synthetic routes employed to obtain the imidazole derivatives are shown in Scheme 1. The parent imidazoles 2-(anthracen-9-yl)-4,5-diphenyl-1*H*-imidazole (**2a**), 4,5-diphenyl-2-(pyren-1-yl)-1*H*-imidazole (**2c**) and 2-(anthracen-9-yl)-1-butyl-4,5-diphenyl-1*H*-imidazole (**3a**) were prepared by reported methods [26,27]. The NMR spectral data matched well with the literature data. Analytical data of the hitherto unknown compounds are compiled here.

#### 2.2.1. General procedure for synthesis of 4,5-diphenyl-2-substituted-1H-imidazoles

A mixture of benzil (2.10 g, 10 mmol), corresponding aldehyde (10 mmol), ammonium acetate (3.08 g, 40 mmol) and acetic acid (20 mL) was heated to reflux for 48 h. After the completion of the reaction, it was poured into ice-cold water to obtain a tan solid. It was recrystallized from dichloromethane and ethanol mixture to yield the analytically pure product.

##### 2.2.1.1. 2-(10-Bromoanthracen-9-yl)-4,5-diphenyl-1H-imidazole (**2b**).

Yellow powder, yield 83%. $^1$H NMR (acetone-$d_6$, 500 MHz): $\delta$ 11.96 (s, 1 H), 8.61 (d, $J$ = 9 Hz, 2 H), 8.06 (d, $J$ = 9 Hz, 2 H), 7.68–7.79 (m, 6 H), 7.58–7.62 (m, 2 H), 7.38 (bs, 6 H). $^{13}$C NMR (acetone-$d_6$, 125 MHz): $\delta$ 142.91, 137.73, 135.68, 132.15, 131.52, 130.12, 128.77, 128.17, 128.12, 127.76, 127.66, 127.57, 127.38, 127.00, 126.70, 126.60, 123.76. HR MS (ESI) $m/z$ calcd. for $C_{29}H_{19}BrN_2$: 474.0732; Found: 474.0721.

#### 2.2.2. General procedure for the butylation of 4,5-diphenyl-2-substituted-1H-imidazoles

A mixture of 4,5-diphenyl-2-substituted-1*H*-imidazole (8 mmol), 1-bromobutane (1.64 g, 12 mmol), BTEAC (0.50 g), 15 mL of 50% sodium hydroxide and benzene (5 mL) (CAUTION: Benzene is a known carcinogen) was refluxed for 36 h. After a clear organic layer formed, the reaction mixture was poured into beaker containing hot water. It was allowed to stand overnight in a hood. The solid formed was collected by filtration and thoroughly wash with liberal amounts of water. Finally, the solid residue was purified by recrystallization with dichloromethane and hexane.

##### 2.2.2.1. 2-(10-Bromoanthracen-9-yl)-1-butyl-4,5-diphenyl-1H-imidazole (**3b**).

Orange crystalline solid, yield 84%. Recently it has been reported that the title compound can also be synthesized by the reaction of 2-(anthracen-9-yl)-1-butyl-4,5-diphenyl-1*H*-imidazole with $Br_2$ in $CS_2$ [26]. $^1$H NMR ($CDCl_3$, 500 MHz): $\delta$ 8.63 (d, $J$ = 8.5 Hz, 2 H), 7.78 (d, $J$ = 8.5 Hz, 2 H), 7.62–7.65 (m, 4 H), 7.50–7.57 (m, 7 H), 7.21–7.24 (m, 2 H), 7.15–7.17 (m, 1 H), 3.45 (t, $J$ = 7.5 Hz, 2 H), 1.00 (quin, $J$ = 7.5 Hz, 2 H), 0.68 (sext, $J$ = 7.5 Hz, 2 H), 0.26 (t, $J$ = 7.5 Hz, 3 H). $^{13}$C NMR ($CDCl_3$, 125 MHz): $\delta$ 142.64, 136.88, 133.43, 131.51, 130.35, 130.00, 129.22, 128.24, 127.99, 127.61, 126.97, 126.11, 125.78, 125.60, 125.25, 125.18, 124.90, 124.33, 43.27, 31.20, 18.08, 11.73.

##### 2.2.2.2. 1-Butyl-4,5-diphenyl-2-(pyren-1-yl)-1H-imidazole (**3c**).

Pale yellow crystalline solid, yield 65%. $^1$H NMR ($CDCl_3$, 500 MHz): $\delta$ 8.29 (d, $J$ = 7.5 Hz, 1 H), 8.21–8.26 (m, 3 H), 8.13–8.18 (m, 4 H), 8.04–8.08 (m, 1 H), 7.64–7.66 (m, 2 H), 7.49–7.56 (m, 5 H), 7.22–7.26 (m, 3 H), 7.15–7.18 (m, 1 H), 3.75 (t, $J$ = 7.5 Hz, 2 H), 1.13 (quin, $J$ = 7.5 Hz, 2 H), 0.77 (sext, $J$ = 7.5 Hz, 2 H), 0.37 (t, $J$ = 7.5 Hz, 3 H). $^{13}$C NMR ($CDCl_3$, 125 MHz): $\delta$ 146.39, 137.58, 134.43, 131.66, 131.39, 130.98, 130.78, 130.64, 130.48, 129.11, 128.83, 128.36, 128.24, 128.03, 128.00, 127.82, 127.08, 126.58, 125.98, 125.94, 125.72, 125.34, 125.26, 124.69, 124.59, 124.28, 44.30, 32.15, 18.95, 12.81. HR MS (ESI) $m/z$ calcd. for $C_{35}H_{28}N_2$: 476.2252; Found: 476.2231.

#### 2.2.3. General procedure for the synthesis of 4,5-diphenyl-1,2-disubstituted imidazoles

A mixture of 1,2-bis(4-methoxyphenyl)ethane-1,2-dione (2.70 g, 10 mmol), the corresponding aldehyde (11 mmol), suitable amine (15 mmol), ammonium acetate (1.54 g, 20 mmol) and acetic acid (20 mL) was refluxed for 48 h. After the completion of the reaction, it was quenched by pouring into ice water. The precipitated solid was filtered and thoroughly washed with water. It was purified by column chromatography on silica gel using dichloromethane-hexane mixture as eluant. Analytically pure samples were obtained by crystallization from dichloromethane and ethanol mixture.

##### 2.2.3.1. 2-(Anthracen-9-yl)-4,5-bis(4-methoxyphenyl)-1-p-tolyl-1H-imidazole (**4a**).

Light yellow powder, yield 72%. $^1$H NMR ($CDCl_3$, 400 MHz): $\delta$ 8.41 (s, 1 H), 7.91–7.93 (m, 2 H), 7.82–7.84 (m, 2 H), 7.62–7.65 (m, 2 H), 7.36–7.43 (m, 4 H), 7.16–7.19 (m, 2 H), 6.79–6.82 (m, 4 H), 6.67 (d, $J$ = 8 Hz, 2 H), 6.55 (d, $J$ = 8 Hz, 2 H), 3.78 (s, 6 H), 1.95 (s, 3 H). $^{13}$C NMR ($CDCl_3$, 125 MHz): $\delta$ 159.10, 158.38, 144.69, 137.86, 137.27, 133.82, 132.24, 132.29, 131.05, 128.88, 128.78, 128.69, 128.57, 128.34, 127.67, 126.84, 126.30, 126.26, 125.64, 125.15, 123.32, 113.97, 113.64, 55.24, 55.15, 20.82. HR MS (ESI) $m/z$ calcd. for $C_{38}H_{30}N_2O_2$: 546.2307; Found: 546.2286.

##### 2.2.3.2. 2-(Anthracen-9-yl)-1,4,5-tris(4-methoxyphenyl)-1H-imidazole (**4b**).

Cream powder, yield 63%. $^1$H NMR ($CDCl_3$, 400 MHz): $\delta$ 8.42 (s, 1 H), 7.92–7.94 (m, 2 H), 7.81–7.83 (m, 2 H), 7.62–7.64 (m, 2 H), 7.37–7.43 (m, 4 H), 7.16–7.19 (m, 2 H), 6.79–6.82 (m, 4 H), 6.70–6.71 (m, 2 H), 6.26–6.29 (m, 2 H), 3.78 (s, 6 H), 3.47 (s, 3 H). $^{13}$C NMR ($CDCl_3$, 125 MHz): $\delta$ 159.09, 158.37, 144.80, 137.77, 132.31, 132.28, 131.06, 129.27, 128.88, 128.69, 128.54, 128.36, 128.17, 127.66, 126.26, 125.60, 125.15, 123.29, 113.97, 113.63, 113.40, 55.24, 55.16, 54.99. HR MS (ESI) $m/z$ calcd. for $C_{38}H_{30}N_2O_3$: 562.2256; Found: 562.2242.

##### 2.2.3.3. 1,4,5-Tris(4-methoxyphenyl)-2-(pyren-1-yl)-1H-imidazole (**4c**).

Colorless solid, yield 74%. $^1$H NMR ($CDCl_3$, 400 MHz): $\delta$ 8.46

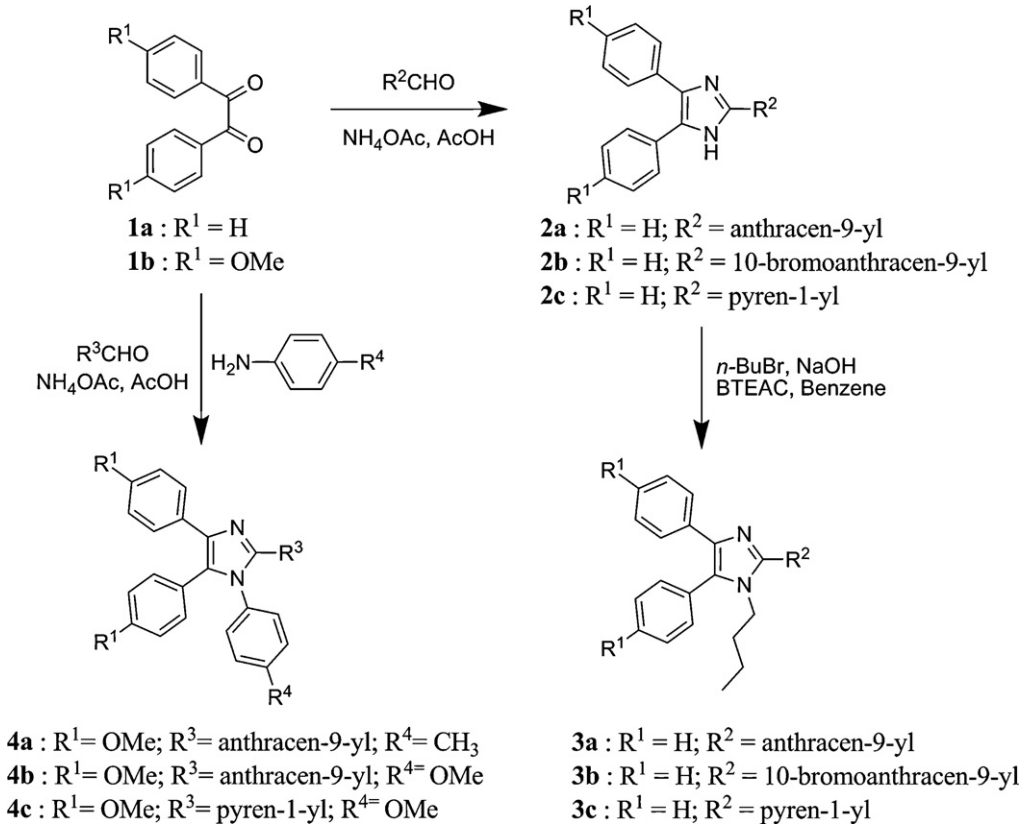


**Scheme 1.** Synthesis of the fluorophore containing imidazoles.

(d, $J$ = 9.2 Hz, 1 H), 8.16–8.18 (m, 2 H), 8.04–8.08 (m, 2 H), 7.98–8.01 (m, 3 H), 7.82 (d, $J$ = 7.9 Hz, 1 H), 7.61–7.64 (m, 2 H), 7.13–7.16 (m, 2 H), 6.79–6.84 (m, 6 H), 6.44–6.48 (m, 2 H), 3.79 (s, 6 H), 3.56 (s, 3 H). $^{13}$C NMR ($CDCl_3$, 125 MHz): $\delta$ 159.15, 158.48, 158.40, 146.33, 137.74, 132.37, 131.41, 131.20, 130.95, 130.87, 129.69, 129.20, 129.01, 128.75, 128.58, 128.06, 127.62, 127.29, 126.04, 125.85, 125.66, 125.33, 124.79, 124.51, 124.02, 123.30, 113.97, 113.65, 55.23, 55.17, 55.12. HR MS (ESI) $m/z$ calcd. for $C_{40}H_{30}N_2O_3$: 586.2256; Found: 586.2244.

### 2.3. Theoretical investigations

The ground state geometry of the compounds at the gas phase were optimized using the density functional theory method with the B3LYP functional in conjugation with the basis set 6-31G(d,p) as implemented in the Gaussian 09 package [28]. The default options for the tight self-consistent field (SCF) convergence and threshold limits in the optimization were used. The electronic transitions were calculated using the time-dependent DFT (B3LYP) theory and the 6-31G (d,p) basis set. At least 10 excited states were calculated for each molecule. Excited-state structures were optimized using configuration interaction singles (CIS) at the same level of theory and fluorescence energies were obtained by using TDDFT by following this procedure. Firstly, the geometry of each imidazole derivative was optimized at its first singlet excited state using CIS/B3LYP/6-31G(d,p). Second, the electronic transitions were calculated by using the CIS optimized excited-state geometry and following TDDFT/B3LYP/6-31G(d,p). Even though the properties calculated for the geometry optimized using a different theory may not be accurate, the trends may be used for meaningful insights. Calculations of the vibrational modes revealed no imaginary frequencies for the final equilibrium geometries.

## 3. Results and discussion

### 3.1. Synthesis and electronic spectra

The synthetic procedures employed for obtaining the fluorophore enriched imidazole derivatives are outlined in Scheme 1. The three-component reaction involving a diketone, an aldehyde and a nitrogen source (ammonium acetate) was performed to obtain the parent imidazoles which were alkylated subsequently by a phase transfer catalytic method. For obtaining the *N*-aryl derivatives, we used the four-component reaction including an additional nitrogen source in the form of aromatic amine besides ammonium acetate. The reaction was smooth with less sterically demanding aniline derivatives; however no *N*-aryl derivatives could be obtained when using 1-naphthylamine or 9-aminoanthracene. Later reactions proceeded to yield the parent *NH*-imidazoles (**2a**–**2c**) rather than the expected *N*-arylated derivatives. The imidazole derivatives containing pyrene or anthracene are yellow in color. The *N*-butylated (**3a**–**3c**) and *N*-arylated (**4a**–**4c**) derivatives are soluble in common organic solvents, while the unsubstituted imidazoles (**2a**–**2c**) are highly soluble in DMF and methanol only.

UV–Vis absorption spectra of the compounds were recorded in a series of solvents of different polarities *viz.* cyclohexane, toluene, dichloromethane, *N,N*-dimethylformamide, acetonitrile and methanol at the concentration of $2 \times 10^{-5}$ M; corresponding data are presented in Table 1. Due to poor solubility, quantitative data for **2c** was gathered in DMF and methanol and for other solvents only qualitative data are presented.

The absorption spectra of the imidazole derivatives recorded in *N,N*-dimethylformamide are displayed in Fig. 1. All the derivatives display a complex absorption profile characteristic of the presence of multiple chromophores. In general, the anthracene based imidazoles exhibit red-shifted absorption when compared to the

**Table 1**
Absorption properties of imidazole derivatives containing anthracene and pyrene.

| Compound | $\lambda_{abs}$, nm ($\varepsilon$, $\times 10^3$ $M^{-1}$ $cm^{-1}$) | | | | | |
|---|---|---|---|---|---|---|
| | Cyclohexane | Toluene | DCM | DMF | ACN | Methanol |
| **2a** | 365 (9.0), 384 (10.9) | 350.5 (5.3), 367.5 (8.4), 387 (9.7) | 368 (9.2), 386.5 (10.4) | 349 (5.5), 368.5 (8.5), 387.5 (9.9) | 365.5 (8.7), 384 (9.7) | 348 (6.3), 364 (9.6), 383 (12.4) |
| **3a** | 348 (5.9), 365 (9.2), 384 (9.9) | 351 (5.5), 368 (8.6), 387 (8.8) | 350.5 (6.5), 368 (9.8), 387 (9.6) | 351.5 (6.1), 368 (9.3), 387.5 (9.2) | 349 (6.1), 366 (9.2), 385 (9.0) | 349 (6.8), 366 (10.0), 385 (9.3) |
| **2b** | 377 (10.5), 397 (13.1) | 361 (5.3), 379.5 (9.2), 400 (10.9) | 360 (6.3), 378.5 (10.6), 398.5 (12.4) | 360.5 (5.2), 379 (8.7), 399 (10.6) | 358 (5.9), 376 (10.0), 396 (11.7) | 356.5 (6.3), 375 (10.5), 395 (11.4) |
| **3b** | 358 (6.4), 377 (10.7), 397 (12.1) | 360.5 (6.2), 379 (10.5), 400 (11.4) | 359.5 (6.8), 378.5 (11.2), 399 (11.9) | 359.5 (6.5), 379 (10.8), 400 (11.7) | 357.5 (7.5), 376.5 (12.2), 397 (13.0) | 357.5 (7.8), 376 (13.1), 397 (13.4) |
| **4a** | 346 (6.3), 364 (9.3), 384 (9.5) | 349.5 (6.0), 367.5 (8.9), 387.5 (8.8) | 350 (6.5), 367.5 (9.6), 387 (9.3) | 349.5 (6.5), 368 (9.6), 387 (9.3) | 332 (3.6), 348.5 (6.3), 366 (9.4), 385 (9.0) | 333 (3.7), 348.5 (6.8), 366 (10.2), 385 (9.4) |
| **4b** | 346.5 (0.07), 364.5 (0.1), 384.5 (0.09) | 349.5 (5.7), 367.5 (8.5), 387 (8.4) | 350 (6.0), 368 (8.9), 387 (8.6) | 349.5 (6.1), 367.5 (9.0), 387 (8.8) | 331.5 (3.5), 348 (5.9), 366 (8.7), 385 (8.4) | 333 (3.3), 348 (6.2), 366 (9.2), 385 (8.5) |
| **2c** | 308, 323, 344, 354[a] | 377[a] | 372[a] | 379 (29.8) | 371[a] | 357.5 (28.9) |
| **3c** | 308 (14.8), 323 (18.0), 342 (23.9) | 327.5 (17.2), 345.5 (24.7) | 328 (20.0), 344 (29.0) | 345 (24.9) | 342 (27.4) | 328 (22.0), 342 (33.0) |
| **4c** | 328 (19.3), 342.5 (18.4), 361.5 (22.3) | 330 (17.8), 359.5 (20.1) | 329 (19.3), 344 (23.2) | 328.5 (18.6), 344 (22.3) | 342 (23.5) | 327 (20.5), 342 (28.1) |

[a] Extinction coefficient could not be obtained due to poor solubility.

analogous pyrene derivatives. However, the molar extinction coefficients of the pyrene derivatives are significantly higher than those observed for the anthracene derivatives.

The anthracene based imidazoles exhibit absorption spectra featuring π–π* transitions arising from the anthracene segment in the range 349–400 nm. This band showed vibrational fine structure characteristic of isolated anthracene chromophore [29,30]. The intensity ratio of the three sharp peaks is typically 1:1.7:1.8. Another interesting feature is that the incorporation of bromine on anthracene unit (**2b** and **3b**) leads to a slight red shift and hyperchromism for the π–π* transition when compared to the non-brominated analogs (**2a** and **3a**). However, the *N*-alkylation of the imidazole unit has no effect on the absorption features of the anthracene based imidazoles.

Pyrene based imidazoles exhibited broad and comparatively less structured absorption profiles. Two absorption bands peaking at ~280 and 328–379 nm were observed. The red-shifted peak is assigned to have major contribution from the π–π* transition while the shorter wavelength absorption may arise from a pyrene localized π–π* transition [31,32]. Interestingly, *N*-alkylation (**3c**) led to a blue-shift for the longer wavelength peak when compared to that of **2c**. Probably, *N*-alkylation inhibits the conjugation extension into the imidazole segment such a reduction in conjugation might blue shift the absorption wavelength [33]. Despite the more pronounced non-planarity between the imidazole and the pyrene segments the red-shifted absorption observed for **4c** clearly indicate the involvement of the phenyl groups in the extension of conjugation by delocalization of π-electrons when compared to the *N*-butyl derivative (**3c**).

The absorption spectra of the compounds were unaffected by the solvent polarity which indicates that the interaction of the dyes with the solvents in the ground state is less significant [34]. A slight blue shift observed for the imidazoles (**2a**, **2b** and **2c**) in ACN and methanol when compared to those recorded in nonpolar solvents such as cyclohexane and toluene probably stems from the hydrogen bonding interactions between the *N*-H unit and the solvents [35].

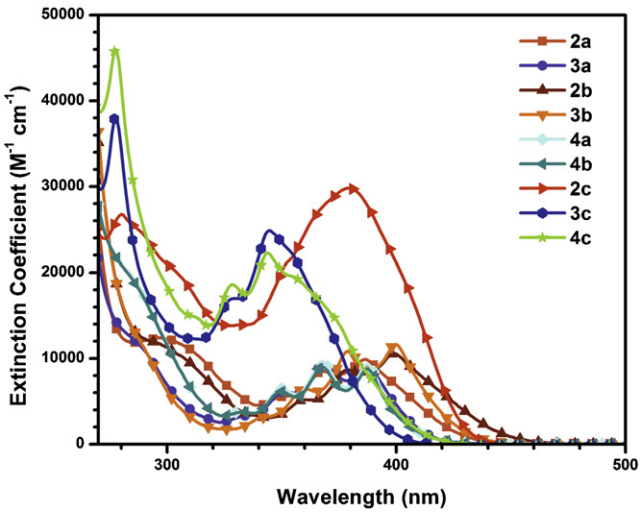


**Fig. 1.** Absorption spectra for the imidazole derivatives (**2a**–**2c**, **3a**–**3c** and **4a**–**4c**) recorded in *N*,*N*-dimethylformamide solutions.

### 3.2. Emission spectra

Emission spectra of the compounds were measured in a series of solvents of different polarities *viz.* cyclohexane, toluene, dichloromethane, *N*,*N*-dimethylformamide, acetonitrile and methanol and the relevant parameters are presented in Table 2. For example, the emission spectra recorded for the compounds in cyclohexane are displayed in Fig. 2. It may be appropriate to discuss the emission spectra of the compounds in three different categories: *N*-H imidazoles, *N*-alkyl imidazoles and *N*-aryl imidazoles. Within a class, the nature of the aryl substituent on the C-2 position plays the major role in positioning the emission peak. Among the anthracene containing imidazoles the *N*-H imidazoles (**2a** and **2b**) show the red-shifted emission when compared to the corresponding *N*-alkyl (**3a** and **3b**) and *N*-aryl (**4a** and **4b**) imidazoles. On the contrary, no such effect was observed for the pyrene containing imidazoles (**2c** and **3c**) and they showed the most blue-shifted emission profile among the series. This is opposite to the trend observed in the absorption spectra (*vide supra*). It may be reasoned that the anthracene containing *N*-H imidazoles (**2a** and **2b**) in the excited state assumes the more planar structure when compared to the *N*-alkyl imidazoles (**3a** and **3b**). Obviously the attainment of planarity is hindered in the latter compounds due to the presence of *N*-alkyl unit. Very large Stokes shifts observed for the compounds **2a** and **2b** when compared to **3b** and **3c** also supports this suggestion. However, as the pyrene based imidazoles

**Table 2**
Emission properties of imidazole derivatives containing anthracene or pyrene segments.

| Dye | $\lambda_{em}$, nm ($\Phi_F$, %) | | | | | | |
|---|---|---|---|---|---|---|---|
| | Cyclohexane | Toluene | DCM | DMF | ACN | MeOH | Film |
| **2a** | 489 (51) | 492 (48) | 495 (58) | 494 (49) | 492 (49) | 475 (52) | [a] |
| **3a** | 433, 453 (50) | 456 (53) | 466 (64) | 482 (44) | 482 (39) | 458 (53) | 467 |
| **2b** | 506 (36) | 510 (33) | 512 (18) | 526 (11) | 515 (6) | 497 (22) | [a] |
| **3b** | 465 (48) | 470 (55) | 490 (48) | 517 (8) | 515 (9) | 483 (28) | 483 |
| **4a** | 459 (53) | 467 (35) | 499 (14) | 524 (6) | 526 (2) | 500 (6) | 450 |
| **4b** | 459 (55) | 467 (33) | 500 (14) | 520 (6) | 498 (7) | 502 (6) | 441 |
| **2c** | 430 (81) | 437, 456 (75) | 458 (76) | 472 (77) | 467 (59) | 457 (76) | [a] |
| **3c** | 432 (86) | 438 (72) | 453 (71) | 463 (73) | 463 (60) | 445 (63) | 461 |
| **4c** | 428,444 (87) | 452 (75) | 477 (69) | 492 (67) | 494 (48) | 477 (59) | 470 |

[a] No emission.

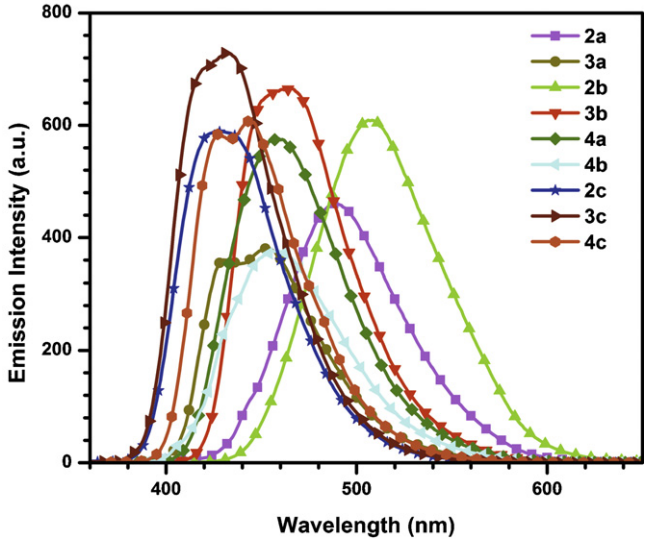


**Fig. 2.** Emission spectra for the imidazole derivatives (**2a**–**2c**, **3a**–**3c** and **4a**–**4c**) recorded in cyclohexane.

are already assuming more planar structure (see below theoretical calculations) structural reorganization is less significant for the pyrene derivatives. A similar reason can also be assigned for the red-shifted emission observed for the *N*-aryl derivative **4c**. In keeping with these observations, the Stokes shift calculated for the *N*-H imidazoles (**2a** and **2b**) containing anthracene moiety are larger than those of the corresponding *N*-alkyl and aryl imidazoles (**3a**, **3b**, **4a** and **4b**). Very large Stokes shifts generally indicate an extensive structural reorganization in the excited state [35]. While for the pyrene based imidazoles a reverse order was noticed. Solvent polarity played no significant role on the emission peak of the *N*-H imidazoles containing anthracene unit (**2a** and **2b**). However, the *N*-alkyl and aryl derivatives (**3a**, **3b**, **4a**, and **4b**) exhibited a positive solvatochromism indicative of a stabilized excited state in the polar solvents. The difference in the behavior of the *N*-substituted derivatives in the excited state may originate from the more dipolar interactions with the solvents. This attribution seems reasonable as the *N*-substituted derivatives (**3a**, **3b**, **4a**, and **4b**) possess larger dipole moment in the ground state than the unsubstituted imidazoles (**2a** and **2b**) (*vide supra*). Interestingly, all the pyrene derivatives (**3a**, **3b** and **3c**) showed a positive solvatochromism. These trends were also manifested in the correlation of Stokes shift with the polarity scale (Table 3). On increasing the polarity of the solvent the Stokes shift increased monotonously except for minor variations observed for the DMF and methanol solutions which may be ascribed to the specific interactions such as hydrogen bonding or molecular aggregations (see below) [36].

The emission of the *N*-H imidazoles (**2a**, **2b** and **2c**) is completely quenched in the solid state and those of *N*-alkyl derivatives are blue shifted when compared to those observed in polar solvents. Emission quenching in the solid state for the *N*-H imidazoles may be attributed to the formation molecular assemblies [37] and the blue shift of the *N*-alkyl derivatives may originate due to the change in the dielectric constant of the medium of measurement [38]. Formation of aggregated dimers in the excited state is more likely as the emission intensity of the *N*-H imidazoles (**2a**–**2c**) dramatically decreased on increasing the concentration in polar solvents such as dimethylformamide (see for example Fig. 3). The solid state photoluminescence maxima of the anthracene based *N*-aryl derivatives (**4a** and **4b**) are blue shifted than those observed in cyclohexane (Figs. 4 and 5 and Table 2) may be attributed to the formation of H-aggregates.

Fluorescence quantum yield was determined by using coumarin-1 as reference ($\Phi_F$ = 0.99 in ethyl acetate) [39,40]. In general, the pyrene based imidazoles (**2c**, **3c** and **4c**) showed emission efficiency higher than those of the anthracene based derivatives (**2a**, **2b**, **3a**, **3b**, **4a**, and **4b**). Also, the quantum yield was significantly affected by the solvent polarity. On increasing the polarity of the solvent, the quantum efficiency decreased dramatically except for in methanol. In methanol, all the derivatives displayed reasonable emission intensity which probably suggests that the emissive states do not involve appreciable charge transfer.

**Table 3**
Stokes shift observed for the imidazole derivatives in different solvents and the parameters used for the correlation.

| Solvent | $E_T(30)$ | $\pi^*$ | Orientation polarizability | Stokes shift ($cm^{-1}$) | | | | | | | | |
|---|---|---|---|---|---|---|---|---|---|---|---|---|
| | | | | **2a** | **3a** | **2b** | **3b** | **4a** | **4b** | **2c** | **3c** | **4c** |
| Cyclohexane | 30.9 | 0.00 | −0.001 | 5592 | 2947 | 5426 | 3684 | 4255 | 4221 | 4993 | 6092 | 4298 |
| Toluene | 33.9 | 0.54 | 0.013 | 5515 | 3910 | 5392 | 3723 | 4393 | 4427 | 3642 | 6113 | 5693 |
| DCM | 40.7 | 0.82 | 0.219 | 5671 | 4381 | 5563 | 4654 | 5800 | 5840 | 5048 | 6995 | 8105 |
| DMF | 43.2 | 0.88 | 0.275 | 5564 | 5060 | 6051 | 5658 | 6756 | 6609 | 4993 | 6092 | 4298 |
| ACN | 45.6 | 0.75 | 0.306 | 5716 | 5227 | 5835 | 5771 | 6963 | 5894 | 5541 | 7641 | 8997 |
| MeOH | 55.4 | 0.60 | 0.309 | 5057 | 4140 | 5196 | 4485 | 5974 | 6054 | 6090 | 6768 | 8275 |

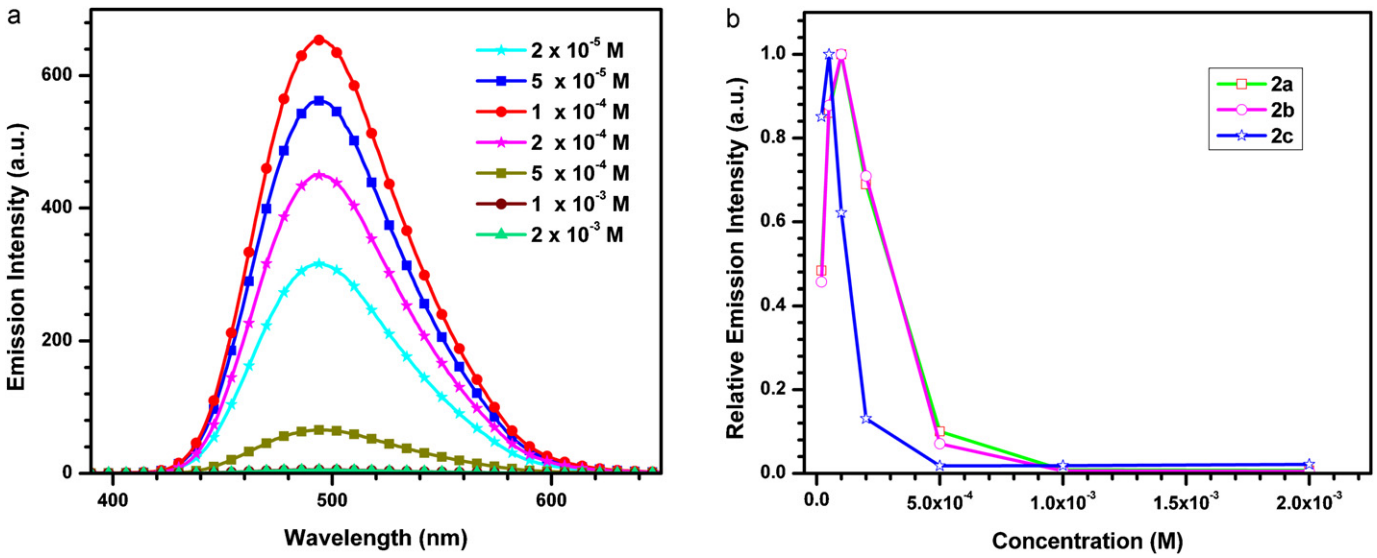


**Fig. 3.** (a) Emission spectra of **2a** recorded in DMF at different concentrations. (b) Variation of emission intensity for **2a–2c** in DMF with concentration.

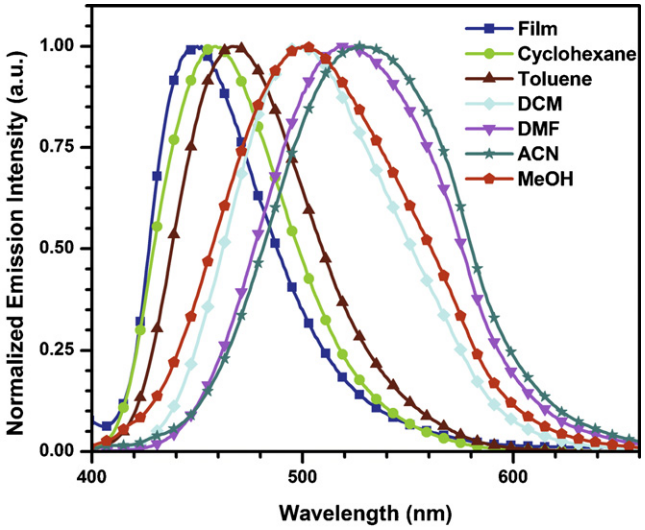


**Fig. 4.** Emission spectra of **4a** recorded in series of solvents and film.

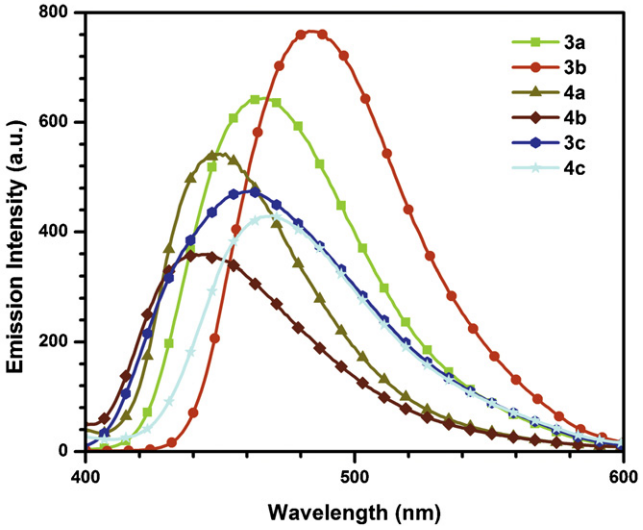


**Fig. 5.** Emission spectra recorded for the spin cast films of **3a–3c** and **4a–4c**.

### 3.3. Solvatochromism

Solvent dependent spectral properties were interpreted with Lippert–Mataga equation [41–43], $E_T(30)$ parameter [44] and Kamlet–Taft equation [45,46]. Lippert–Mataga equation provides a measure for the change in the dipole moment upon excitation of molecule. In this method a plot of Stokes' shift versus orientation polarizability ($\Delta f$) was performed to fit the equation given below

$$\bar{\nu}_A - \bar{\nu}_F = \frac{2}{hc}\left(\frac{\varepsilon - 1}{2\varepsilon + 1} - \frac{n^2 - 1}{2n - 1}\right)\frac{(\mu_E - \mu_G)^2}{a^3} + \text{constant}$$

where $h$ is Planck's constant ($6.6256 \times 10^{-27}$ erg), $c$ is the velocity of light ($2.9979 \times 10^{10}$ cm/s), $a$ is radius of cavity in which molecule resides, $\bar{\nu}_A$ and $\bar{\nu}_F$ are the wave numbers ($cm^{-1}$) of the absorption and emission, respectively; $\varepsilon$ is dielectric constant and $n$ is refractive index of the solvent. The orientation polarizability is defined as

$$\Delta f = \frac{2}{hc}\left(\frac{\varepsilon - 1}{2\varepsilon + 1} - \frac{n^2 - 1}{2n - 1}\right)$$

Representative plots showing the variation of Stokes shift with orientation polarizability for the compounds **2a**, **2c** and **4c** are shown in Fig. 6. Anthracene derivatives (**2a**, **2b**, **3a**, **3b** and **4a**) showed deviations from linearity in methanol while the pyrene derivatives (**2c**, **3c** and **4c**) deviated from linearity in cyclohexane or dimethylformamide. The anomalous behavior of the anthracene containing dyes in methanol clearly indicates the presence of non-specific interactions such as hydrogen bonding or molecular aggregation and it must be noted here that the Lippert–Mataga correlation does not account for the hydrogen bonding effects and formation of molecular complexes. Since the π–π interactions are generally facilitated in the non-polar solvents such as cyclohexane, the deviation observed for **2c** in cyclohexane may be attributed to the aggregation of the dye molecules by hydrogen bonding or stacking interactions is speculated.

The plot of Stokes shifts versus the $E_T(30)$ parameter shown for **2c** and **3a** in Fig. 7 confirmed the exhibition of positive solvatochromism by the compounds. Again the anthracene based imidazoles (**2a**, **2b**, **3a**, **3b**, **4a** and **4b**) deviated significantly in methanol while the pyrene containing imidazoles (**2c**, **3c** and **4c**) showed deviation for cyclohexane or methanol and dimethylformamide. Even though this correlation effectively maps the charge

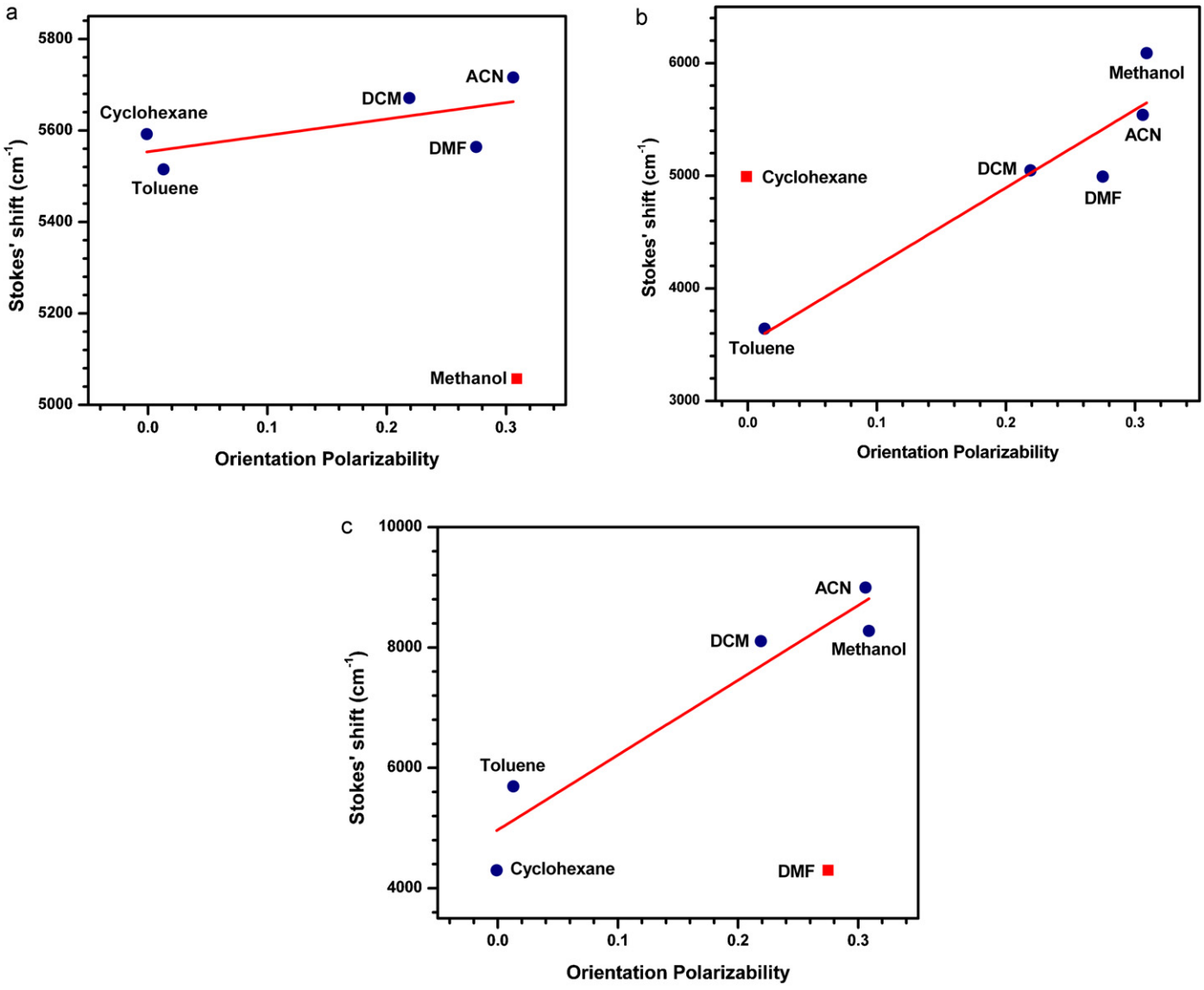


**Fig. 6.** Lippert–Mataga plots of the dyes (a) **2a**, (b) **2c** and (c) **4c**.

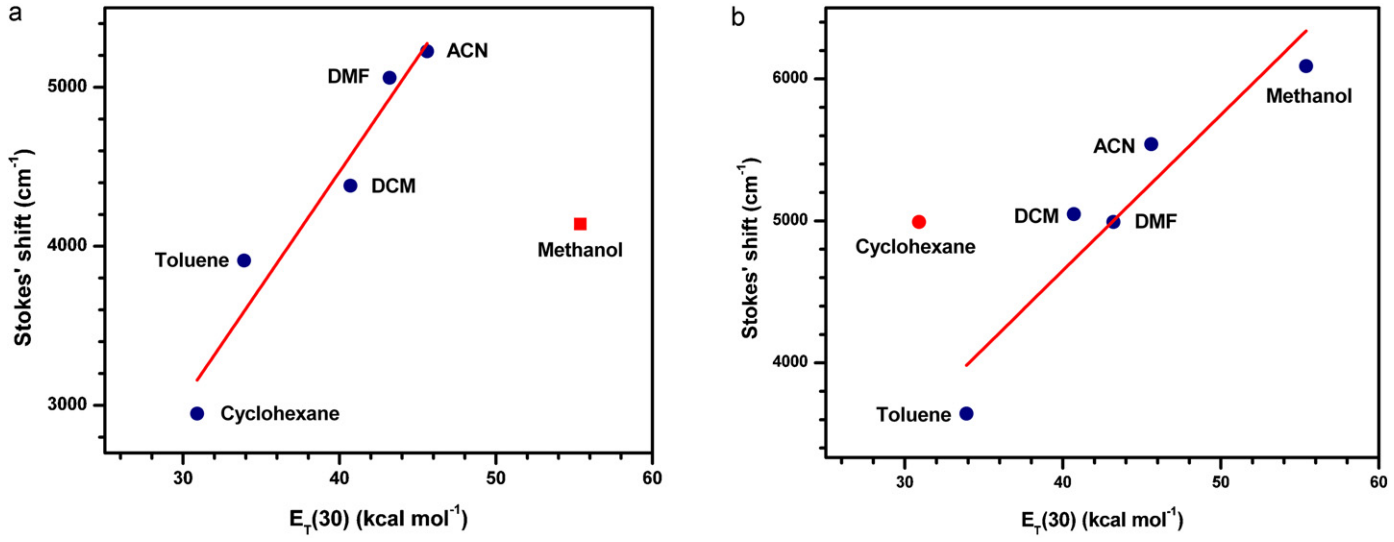


**Fig. 7.** Correlation of $E_T(30)$ parameter with Stokes shift for the compounds (a) **2c** and (b) **3a**.

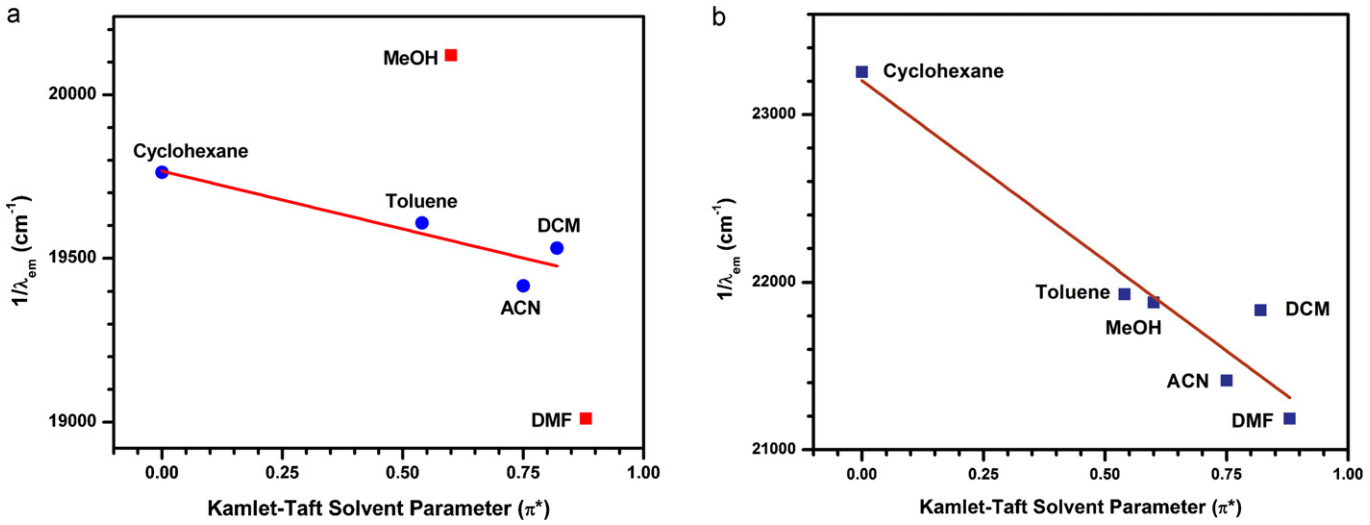


**Fig. 8.** Kamlet–Taft plots for the compounds (a) **2b** and (b) **2c**.

transfer in a molecule with the range of solvents, the polarizability in protic solvents is often misinterpreted. For this reason the Stokes shift observed in methanol or dimethylformamide did not fall in the straight line. The deviation observed for **2c** in cyclohexane again reiterates the formation of aggregates.

Finally, the emission maxima observed in the different solvents were plotted against Kamlet–Taft solvent parameter ($\pi^*$). Selected trends observed for **2b** and **2c** is shown in Fig. 8. The Kamlet–Taft solvent parameters are the hydrogen bond donation ability $\alpha$, hydrogen bond acceptor ability $\beta$ and the dipolarity-polarizability $\pi^*$; the linear equation relating the Kamlet–Taft parameters with the emission maximum is generalized as

$$\bar{\nu}_f^{\max} = 23.36 - 6.70\pi^* - 0.64\alpha + 0.54\beta$$

Strikingly, the Kamlet–Taft plots showed better linear fit for the pyrene containing derivatives **2c**, **3c** and **4c**. Because this scale accounts hydrogen bonding interactions also, it may be safely assumed that deviations observed for these derivatives in the correlations of orientation polarizability and $E_T(30)$ arise mainly due to hydrogen bonding interactions. As the NH imidazole **2c** showed anomalous behavior for the earlier correlations in cyclohexane it is suggested to be arising from the intermolecular hydrogen bonding while in **3c** and **4c** it is due to the hydrogen bonding interactions with the solvents However, the anthracene containing derivatives (**2a**, **2b**, **3a**, **3b**, **4a** and **4b**) displayed scattering in polar solvents such as methanol, acetonitrile and dimethylformamide indicating a molecular aggregation which is not modeled in these correlations.

From the above discussion it is clearly evident that in these molecules besides the solvent parameters such as polarity and polarizability the secondary effects such as hydrogen bonding or molecular aggregation affects the emission properties. Thus, the non-specific interactions between the dye molecules and the solvents or neighboring molecules significantly alter the relaxation of molecules in the excited states.

### 3.4. Theoretical studies

To gain more insight into the photophysical behavior of the imidazole derivatives, DFT calculations were performed for the compounds. The unconstrained geometries of the compounds in gas phase were optimized by DFT using the Becke's three-parameter functional hybridized with the Lee–Yang–Parr correlation functional and the 6-31G(d,p) basis set. Optimized geometries of the anthracene derivatives (**2a**, **3a** and **4a**) showed

**Table 4**
Calculated inter-planar angles (°) formed by imidazole unit with other aromatic segments in the optimized geometries of the compounds.

| Compound | Ground state (DFT/B3LYP/6-31G(d,p)) | | | | Excited state (CIS/B3LYP/6-31G(d,p)) | | | |
|---|---|---|---|---|---|---|---|---|
| | *C*-Phenyl | *C*-Phenyl | *N*-Phenyl | Anthracene/pyrene | *C*-Phenyl | *C*-Phenyl | *N*-Phenyl | Anthracene/pyrene |
| **2a** | 27.98 | 40.71 | NA | 51.27 | 38.21 | 41.47 | NA | 33.26 |
| **3a** | 20.71 | 62.79 | NA | 70.23 | 28.70 | 64.77 | NA | 65.06 |
| **4b** | 24.05 | 55.39 | 61.65 | 75.55 | 30.15 | 61.58 | 64.67 | 69.42 |
| **2c** | 28.97 | 40.57 | NA | 28.01 | 40.85 | 34.36 | NA | 9.28 |
| **3c** | 20.55 | 68.00 | NA | 53.94 | 28.46 | 72.78 | NA | 37.42 |
| **4c** | 25.43 | 55.68 | 61.81 | 45.78 | 31.65 | 60.10 | 64.82 | 30.78 |

**Table 5**
Computed dipole moments, absorption (TDDFT/B3LYP/6-31G(d,p)) and emission wavelengths (CIS/B3LYP/6-31G(d,p)//TDDFT B3LYP/6-31G(d,p)), oscillator strengths and Stokes shifts of the compounds.

| Compound | $\mu_g$, Debye | $\lambda_{abs}$, nm | $f$ | Assignment | $\mu_e$, Debye | $\lambda_{em}$, nm | Stokes shift, $cm^{-1}$ |
|---|---|---|---|---|---|---|---|
| **2a** | 3.20 | 431.6 | 0.20 | HOMO → LUMO (96%) | 2.90 | 520.6 | 3961 |
| **3a** | 4.19 | 429.1 | 0.10 | HOMO → LUMO (92%) HOMO-1 → LUMO (8%) | 4.07 | 465.1 | 1804 |
| **4b** | 4.41 | 458.9 | 0.01 | HOMO → LUMO (99%) | 4.58 | 481.0 | 1001 |
| **2c** | 2.99 | 405.1 | 0.64 | HOMO → LUMO (95%) | 2.73 | 445.9 | 2259 |
| **3c** | 4.10 | 391.2 | 0.29 | HOMO → LUMO (88%)HOMO-1 → LUMO (10%) | 4.00 | 416.3 | 1541 |
| **4c** | 4.63 | 420.2 | 0.28 | HOMO → LUMO (96%) | 4.98 | 444.2 | 1285 |

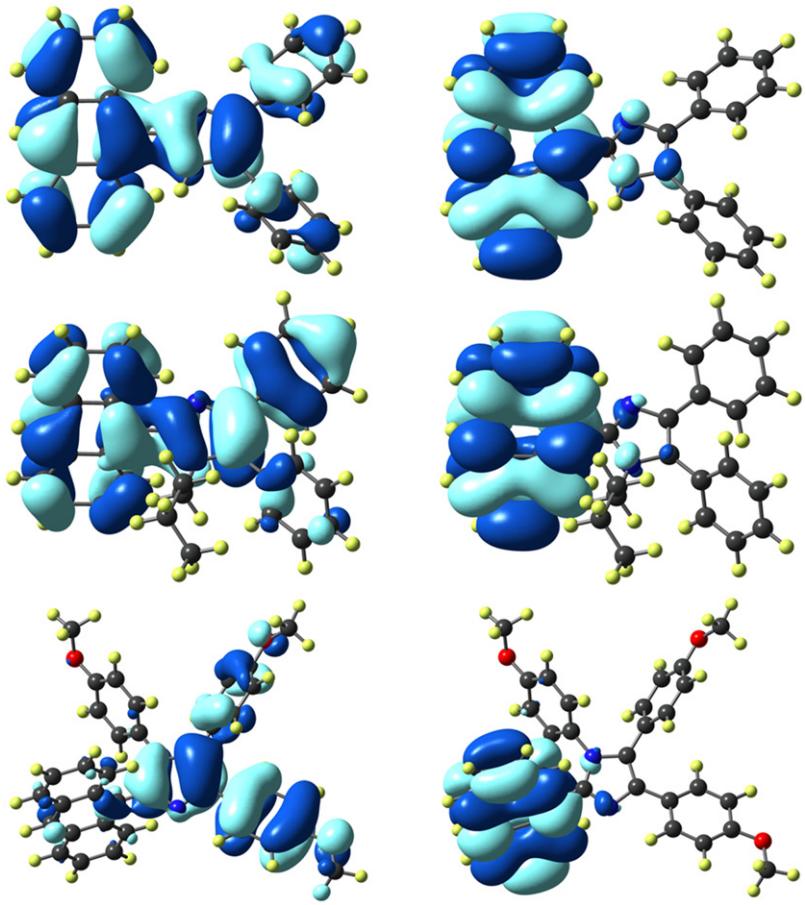

**Fig. 9.** Frontier molecular orbitals (HOMO: left; LUMO: right) of the compounds **2a** (top), **3a** (middle) and **4b** (bottom).

significant deviation from co-planarity between the anthracene and the imidazole rings (Table 4), while in the pyrene derivatives (**2c**, **3c** and **4c**) pyrene unit was less tilted from the imidazole plane (Table 4). The non-planarity between the imidazole and the anthracene/pyrene units increased on *N*-substitution of the imidazole. In the excited state *N*-H imidazoles (**2a** and **3a**) assumed more planar configuration between the imidazole and the anthracene or pyrene unit. It is also notable that among the anthracene and pyrene derivatives (**2a**, **3c**, **3a** and **3c**), the pyrene containing imidazoles (**3a** and **3c**) formed relatively more planar arrangement between the imidazole and the aromatic segments. Another interesting feature is the negligible change in the dipole moment for the dyes in the gaseous excited state. This points that the structure in the excited state is less polarized when compared to that in the ground state. This is quite reasonable as there are no trivial donor–acceptor structural elements in the present structures. However, the positive solvatochromism observed for all the compounds suggests a more polarized excited state. This must result in a higher dipole moment in the excited state. The disagreement between the computed dipole moments of the dyes in the gaseous phase and the observed positive solvatochromism probably points that the solvation and the induced dipole moments of the dyes play a major role in dictating the excited state properties of the dyes in solution phase.

The lowest unoccupied molecular orbital (LUMO) of the compounds were invariably localized on the anthracene or pyrene unit (Figs. 9 and 10). The highest occupied molecular orbital of the compounds were generally contributed by the entire molecule with the exception of **4b** in which the anthracene unit did not participate in the LUMO construction. The calculated ground state dipole moment increased on *N*-substitution which suggests stronger donor ability for the imidazole on *N*-substitution (Table 5). Although the

**Table 6**
Thermal and electrochemical properties of imidazole derivatives.

| Compound | $T_d$ (°C) | $T_{onset}$ (°C)[a] | $E_{ox}$ (V) | HOMO (eV) | $E_{0-0}$ | LUMO (eV) |
|---|---|---|---|---|---|---|
| **2a** | 450 | 376 | 1.036 | 5.836 | 2.86 | 2.976 |
| **3a** | 432 | 355 | 1.176 | 5.976 | 2.96 | 3.016 |
| **2b** | 422 | 318 | 1.084 | 5.884 | 2.76 | 3.124 |
| **3b** | 347 | 344 | 1.244 | 6.044 | 2.86 | 3.184 |
| **4a** | 430 | 370 | 1.168, 1.068 | 5.868 | 2.91 | 3.058 |
| **4b** | 430 | 343 | 1.156, 1.060 | 5.860 | 2.90 | 3.056 |
| **2c** | 416 | 367 | 0.468 | 5.268 | 2.96 | 2.308 |
| **3c** | 460 | 393 | 1.132, 0.724 | 5.524 | 3.09 | 2.842 |
| **4c** | 473 | 428 | 1.012, 0.580 | 5.380 | 2.97 | 2.842 |

[a] Temperature corresponding to 10% weight loss.

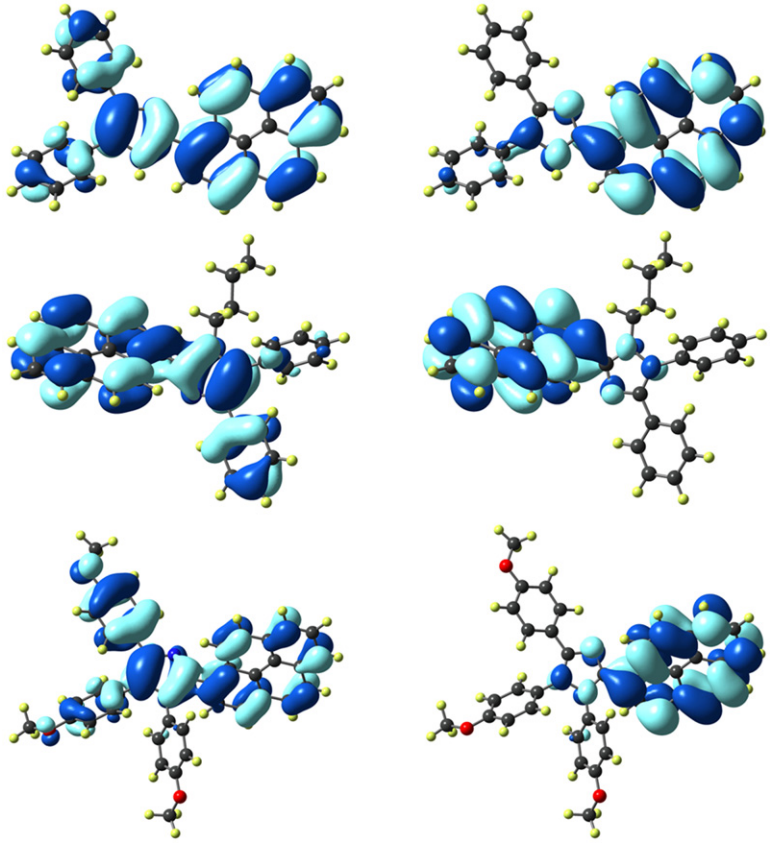

**Fig. 10.** Frontier molecular orbitals (HOMO: left; LUMO: right) of the compounds **2c** (top), **3c** (middle) and **4c** (bottom).

trend in the lowest energy electronic excitations experimentally observed for the compounds are consistent with the calculated ones, their oscillator strengths and absorption positions vary significantly. Such deviations may be arising due to the long range intermolecular interactions or solvent specific contributions which cannot be treated effectively by TDDFT alone [47]. The trend in the emission peak positions calculated by the theory for the compounds **2a** and **3a** follows grossly the trend exhibited by the dyes in the solution. But for the compounds **2c** and **3c** the same trend predicted by theory for the emission peak is not realized in cyclohexane. It may be due to the broadening (see Fig. 2) of the emission profile which led to the incorrect estimation of the emission position. It may be possible that the poorly resolved vibronic pattern contributed to the broadening of the emission profile.

### 3.5. Thermal studies

The thermal stability of the imidazole derivatives was examined by thermogravimetric analysis and the relevant data are presented in Fig. 11 and Table 6. All compounds showed excellent thermal stability and their thermal decomposition temperatures are in the range 347–473. The lowest $T_d$ is observed for **3d** and the highest for **4c**. In general, the pyrene derivatives are more thermally stable than the corresponding anthracene analogs. Pronounced thermal stability for the pyrene based organic amorphous materials is well documented in the literature [48,49]. Among the anthracene imidazoles, the highest thermal stability was observed for the *N*-H imidazole (**2a**). Alkylation (**3a** and **3b**) and arylation (**4a** and **4c**) diminishes the thermal decomposition temperature slightly. But, in the case of pyrene based imidazoles the thermal stability assumes the reverse order **2c** < **3c** < **4c**.

### 3.6. Electrochemical study

The electrochemical propensity of the derivatives was examined by using cyclic voltammetric (CV) and differential pulse voltammetric (DPV) techniques. The redox potentials were calibrated using ferrocene as internal standard in each measurement. The data are collected in Table 6. All the compounds showed one irreversible oxidation peak. However, **4a**, **4b** and **3c** displayed two irreversible oxidation peaks and **4c** exhibited two quasi-reversible peaks. It appears that the electron-rich methoxy and pyrene segments

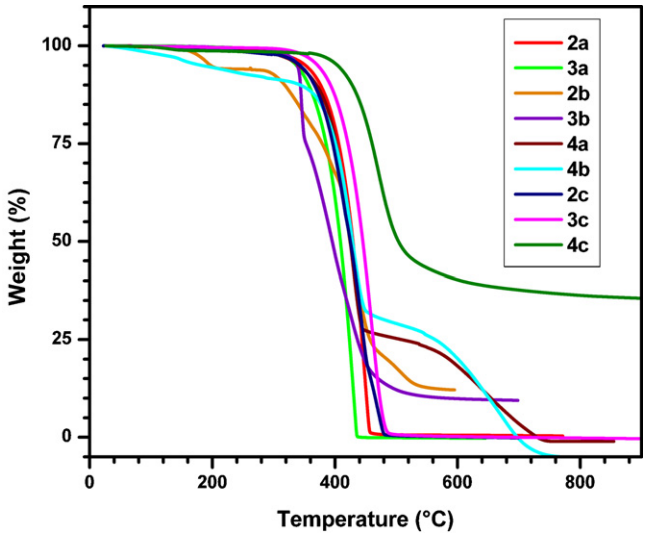


**Fig. 11.** Thermogravimetric traces of the compounds.

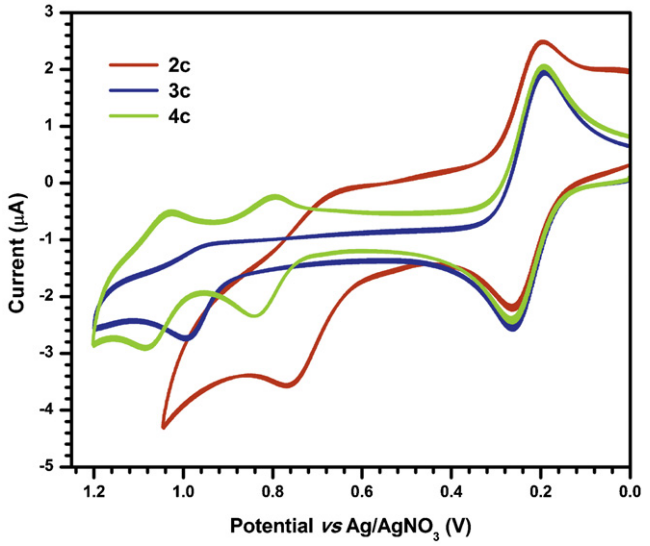


**Fig. 12.** Cyclic voltammograms of pyrene based imidazoles (**2c**, **3c** and **4c**) recorded for dichloromethane solutions.

increase the oxidation ability of the corresponding derivatives (**2c**, **3c**, and **4c**) and they show more anodically shifted redox potentials. Representative cyclic voltammograms of the pyrene derivatives are shown in Fig. 12. The energy of HOMO of these derivatives was calculated by using ferrocene as a reference (4.8 eV) and ranges from 5.27 to 6.04 eV. The HOMO energies within a class of compounds assumed the following order: *N*-unsubstituted (**2a**) < *N*-arylated (**4a**) < *N*-alkylated (**3a**). The LUMO energy was calculated from HOMO energy and band gap derived from the absorption edge and ranges from 2.31 to 3.18 eV. The raised HOMO and lowered LUMO levels observed for the derivative **2c** suggest that it can be a potential candidate for hole-transporting layer.

## 4. Conclusions

In summary, we have synthesized a series of imidazole derivatives containing anthracene and pyrene segments and thoroughly characterized by spectral (NMR, absorption and emission), thermal and electrochemical methods. It was observed that the absorption and emission features of these fluorescent dyes are highly dependent on the conjugation between the imidazole and the anthracene/pyrene segments. The conjugation between these units is modulated by the nature of the *N*-substituents. In case of anthracene derivatives there is no effective conjugation between the imidazole and the anthracene segments due to the deviation from planarity. On the contrary in pyrene derivatives the conjugation is facilitated by the approximately planar configuration between the imidazole and the pyrene segments, however, it is disturbed by the introduction of alkyl or aryl substituent in the imidazole nitrogen. Extended conjugation due to the more planar structural arrangement of imidazole and anthracene/pyrene/phenyl segments leads to the red-shifted absorption and emission profiles in these systems. These results may be useful to design imidazole dyes with higher wavelength absorptions for photovoltaic applications.

## Acknowledgments

We thank the Council of Scientific and Industrial Research (CSIR), New Delhi for financial support (grant no. 01(2111)/07/EMR-II). DK acknowledges CSIR for the research fellowship award.

## Appendix A. Supplementary data

Supplementary data associated with this article can be found, in the online version, at doi:10.1016/j.jphotochem.2010.12.018.

## References

[1] F. Bellina, S. Cauteruccio, S. Montib, R. Rossi, Novel imidazole-based combretastatin A-4 analogues: evaluation of their in vitro antitumor activity and molecular modeling study of their binding to the colchicine site of tubulin, Bioorg. Med. Chem. 16 (2006) 5757–5762.
[2] J.Z. Vlahakis, M. Humb, M.N. Rahman, Z. Jia, K. Nakatsu, W.A. Szarek, Synthesis and evaluation of imidazole-dioxolane compounds as selective heme oxygenase inhibitors: effect of substituents at the 4-position of the dioxolane ring, Bioorg. Med. Chem. 17 (2009) 2461–2475.
[3] K. Bhandari, N. Srinivas, V.K. Marrapu, A. Verma, S. Srivastava, S. Gupta, Synthesis of substituted aryloxy alkyl and aryloxy aryl alkyl imidazoles as antileishmanial agents, Bioorg. Med. Chem. Lett. 20 (2010) 291–293.
[4] F. D'Anna, S. Marullo, R. Noto, Ionic liquids/[bmim][$N_3$] mixtures: promising media for the synthesis of aryl azides by $S_NAr$, J. Org. Chem. 73 (2008) 6224–6228.
[5] C.K. Yerneni, V. Pathak, A.K. Pathak, Imidazolium cation supported solution-phase assembly of homolinear α(1 → 6)-linked octamannoside: an efficient alternate approach for oligosaccharide synthesis, J. Org. Chem. 74 (2009) 6307–6310.
[6] C.M. Lee, H.J. Jeong, S.T. Lim, M.H. Sohn, D.W. Kim, Synthesis of iron oxide nanoparticles with control over shape using imidazolium-based ionic liquids, ACS Appl. Mater. Interfaces 2 (2010) 756–759.
[7] C. Coll, J.V.R. Lis, R.M. Máñez, M.D. Marcos, F. Sancenón, J. Soto, A new approach for the selective and sensitive colorimetric detection of ionic surfactants in water, J. Mater. Chem. 20 (2010) 1442–1451.
[8] X. Chen, S. Kang, M.J. Kim, J. Kim, Y.S. Kim, H. Kim, et al., Thin-film formation of imidazolium-based conjugated polydiacetylenes and their application for sensing anionic surfactants, Angew. Chem. Int. Ed. 49 (2010) 1422–1425.
[9] Z. Fang, S. Wang, L. Zhao, Z. Xu, J. Ren, X. Wang, et al., A novel polymerizable imidazole derivative for blue light-emitting material, Mater. Lett. 61 (2007) 4803–4806.
[10] Z. Ge, T. Hayakawa, S. Ando, M. Ueda, T. Akiike, H. Miyamoto, et al., Solution-processible bipolar triphenylamine-benzimidazole derivatives for highly efficient single-layer organic light-emitting diodes, Chem. Mater. 20 (2008) 2532–2537.
[11] M.Y. Lai, C.H. Chen, W.S. Huang, J.T. Lin, T.H. Ke, L.Y. Chen, et al., Benzimidazole/amine-based compounds capable of ambipolar transport for application in single-layer blue-emitting OLEDs and as hosts for phosphorescent emitters, Angew. Chem. Int. Ed. 47 (2008) 581–585.
[12] Z. Fang, S. Wang, L. Zhao, Z. Xu, J. Ren, X. Wang, et al., Synthesis and characterization of blue light emitting materials containing imidazole, Mater. Chem. Phys. 107 (2008) 305–309.
[13] C.H. Chen, W.S. Huang, M.Y. Lai, W.C. Tsao, J.T. Lin, Y.H. Wu, et al., Versatile, benzimidazole/amine-based ambipolar compounds for electroluminescent applications: single-layer, blue, fluorescent OLEDs, hosts for single-layer, phosphorescent OLEDs, Adv. Funct. Mater. 19 (2009) 2661–2670.
[14] R.Y.C. Shin, T. Kietzke, S. Sudhakar, A. Dodabalapur, Z.K. Chen, A. Sellinger, N-type conjugated materials based on 2-vinyl-4,5-dicyanoimidazoles and their use in solar cells, Chem. Mater. 19 (2007) 1892–1894.
[15] M.S. Tsai, Y.C. Hsu, J.T. Lin, H.C. Chen, C.-P. Hsu, Organic dyes containing *1H*-phenanthro[9,10-d]imidazole conjugation for solar cells, J. Phys. Chem. C 111 (2007) 18785–18793.
[16] Y.T. Chang, S.L. Hsu, G.Y. Chen, M.H. Su, T.A. Singh, E.W.G. Diau, et al., Intramolecular donor–acceptor regioregular poly(3-hexylthiophene)s presenting octylphenanthrenyl-imidazole moieties exhibit enhanced charge transfer for heterojunction solar cell applications, Adv. Funct. Mater. 18 (2008) 2356–2365.
[17] Y.T. Chang, S.L. Hsu, M.H. Su, K.H. Wei, Intramolecular donor–acceptor regioregular poly(hexylphenanthrenyl-imidazole thiophene) exhibits enhanced hole mobility for heterojunction solar cell applications, Adv. Funct. Mater. 21 (2009) 2093–2097.
[18] M. Velusamy, Cha.Y. Hsu, J.T. Lin, C.W. Chang, C.P. Hsu, 1-Alkyl-*1H*-imidazole-based dipolar organic compounds for dye-sensitized solar cells, Chem. Asian J. 5 (2010) 87–96.
[19] M.A. Winnik, S.M. Bystryak, Z. Liu, J. Siddiqui, Synthesis and characterization of pyrene-labeled poly(ethylenimine), Macromolecules 31 (1998) 6855–6864.
[20] S. Zheng, J. Shi, Novel blue-light-emitting polymers containing dinaphthylanthracene moiety, Chem. Mater. 13 (2001) 4405–4407.
[21] J. Shi, C.W. Tang, Anthracene derivatives for stable blue-emitting organic electroluminescence devices, Appl. Phys. Lett. 80 (2002) 3201–3203.
[22] Y. Kan, L. Wang, L. Duan, Y. Hu, G. Wu, Y. Qiu, Highly-efficient blue electroluminescence based on two emitter isomers, Appl. Phys. Lett. 84 (2004) 1513–1515.
[23] M.T. Lee, H.H. Chen, C.H. Liao, C.H. Tsai, Stable styrylamine-doped blue organic electroluminescent device based on 2-methyl-9,10-di(2-naphthyl)anthracene, Appl. Phys. Lett. 85 (2004) 3301–3303.
[24] P. Raghunath, M.A. Reddy, C. Gouri, K. Bhanuprakash, V.J. Rao, Electronic properties of anthracene derivatives for blue light emitting electroluminescent layers

in organic light emitting diodes: a density functional theory study, J. Phys. Chem. A 110 (2006) 1152–1162.
[25] J.R. Lakowicz, Principles of Fluorescence Spectroscopy, 3rd ed., Springer, New York, 2006.
[26] Y.N. Yan, D.Y. Lin, W.L. Pan, X.L. Li, Y.Q. Wan, Y.L. Mai, et al., Synthesis and optical behaviors of 2-(9-phenanthrenyl)-, 2-(9-anthryl)-, and 2-(1-pyrenyl)-1-alkylimidazole homologues, Spectrochim. Acta A 74 (2009) 233–242.
[27] H. Miyasaka, Y. Satoh, Y. Ishibashi, S. Ito, Y. Nagasawa, S. Taniguchi, et al., Ultrafast photodissociation dynamics of a hexaarylbiimidazole derivative with pyrenyl groups: dispersive reaction from femtosecond to 10 ns time regions, J. Am. Chem. Soc. 131 (2009) 7256–7263.
[28] M.J. Frisch, G.W. Trucks, H.B. Schlegel, G.E. Scuseria, M.A. Robb, J.R. Cheeseman, et al., Gaussian 09, Revision A.1, Gaussian, Inc., Wallingford, CT, 2009.
[29] K. Danel, T.H. Huang, J.T. Lin, Y.T. Tao, C.H. Chuen, Blue-emitting anthracenes with end-capping diarylamines, Chem. Mater. 14 (2002) 3860–3865.
[30] I.B. Berlman, Handbook of Fluorescence Spectra of Aromatic Molecules, 2nd ed., Academic Press, New York, 1971.
[31] B.C. Wanga, J.C. Changa, H.C. Tsoa, H.F. Hsua, C.Y. Cheng, Theoretical investigation the electroluminescence characteristics of pyrene and its derivatives, J. Mol. Struct. Theochem. 629 (2003) 11–20.
[32] K.R. Wee, H.C. Ahn, H.J. Son, W.S. Han, J.E. Kim, D.W. Cho, et al., Emission color tuning and deep blue dopant materials based on 1,6-bis(N-phenyl-p-(R)-phenylamino)pyrene, J. Org. Chem. 74 (2009) 8472–8475.
[33] J.S. Yang, C.K. Lin, A.M. Lahoti, C.K. Tseng, Y.H. Liu, G.H. Lee, et al., Effect of ground-State twisting on the trans → cis photoisomerization and TICT state formation of aminostilbenes, J. Phys. Chem. A 113 (2009) 4868–4877.
[34] U. Subuddhi, S. Haldar, S. Sankararaman, A.K. Mishra, Photophysical behaviour of 1-(4-N,N-dimethylaminophenylethynyl)pyrene (DMAPEPy) in homogeneous media, Photochem. Photobiol. Sci. 5 (2006) 459–466.
[35] H. Detert, V. Schmitt, Acidochromism of stilbenoid chromophores with a *p*-aminoaniline centre, J. Phys. Org. Chem. 19 (2006) 603–607.
[36] S.K. Dogra, Spectral characteristics of 2-(3,5-diaminophenyl)benzothiazole: effects of solvents and acid–base concentrations, J. Photochem. Photobiol. A 172 (2005) 185–195.
[37] W. Yan, X. Wan, Y. Chen, Phenalenyl-based boron–fluorine complexes: synthesis, crystal structures and solid-state fluorescence properties, J. Mol. Struct. 968 (2010) 85–88.
[38] K.R.J. Thomas, J.T. Lin, Y.T. Tao, C.W. Ko, Light-emitting carbazole derivatives: potential electroluminescent materials, J. Am. Chem. Soc. 123 (2001) 9404–9411.
[39] J.N. Demas, G.A. Crosby, Measurement of photoluminescence quantum yields, J. Phys. Chem. 75 (1971) 991–1024.
[40] G. Jones II, W.R. Jackson, C.Y. Choi, W.R. Bergmark, Solvent effects on emission yield and lifetime for coumarin laser dyes: requirements for a rotator decay mechanism, J. Phys. Chem. 89 (1985) 294–300.
[41] B. Valeur, Molecular Fluorescence: Principles and Applications, WILEY-VCH Verlag GmbH, Weinheim, 2002.
[42] M. Jozefowicz, J.R. Heldt, Dipole moments studies of fluorenone and 4-hydroxyfluorenone, Spectrochim. Acta A 67 (2007) 316–320.
[43] G.V. Loukova, A.A. Milov, V.P. Vasiliev, V.A. Smirnov, Dipole moment of a metallocene precatalyst in the ground and excited states, Russ. Chem. Bull. Int. Ed. 57 (2008) 1166–1171.
[44] C. Reichardt, Solvatochromic dyes as solvent polarity indicators, Chem. Rev. 94 (1994) 2319–2358.
[45] M.J. Kamlet, J.L.M. Abboud, M.H. Abraham, R.W. Taft, Linear solvation energy relationships. 23. A comprehensive collection of the solvatochromic parameters, $\pi^*$, $\alpha$, and $\beta$, and some methods for simplifying the generalized solvatochromic equation, J. Org. Chem. 48 (1983) 2877–2887.
[46] J.M. Lee, S. Ruckes, J.M. Prausnitz, Solvent polarities and Kamlet–Taft parameters for ionic liquids containing a pyridinium cation, J. Phys. Chem. B 112 (2008) 1473–1476.
[47] A. Dreuw, M. Head-Gordon, Single-reference ab initio methods for the calculation of excited states of large molecules, Chem. Rev. 105 (2005) 4009–4037.
[48] C. Tang, F. Liu, Y.J. Xia, J. Lin, L.H. Xie, G.Y. Zhong, et al., Fluorene-substituted pyrenes-Novel pyrene derivatives as emitters in nondoped blue OLEDs, Org. Electron. 7 (2006) 155–162.
[49] C. Tang, F. Liu, Y.J. Xia, L.H. Xie, A. Wei, S.B. Li, et al., Efficient 9-alkylphenyl-9 pyrenylfluorene substituted pyrene derivatives with improved hole injection for blue light-emitting diode, J. Mater. Chem. 16 (2006) 4074–4080.